


Dynamics of radio-photoluminescence and thermally-stimulated luminescence in KBr:Sm

Go Okada¹  · Yutaka Fujimoto² · Hironori Tanaka² · Safa Kasap³ · Takayuki Yanagida¹

Received: 2 May 2017 / Accepted: 6 July 2017 / Published online: 14 July 2017
© Springer Science+Business Media, LLC 2017

Abstract Sm-doped KBr single crystals were prepared by the Bridgman–Stockbarger technique. The samples show both radio-photoluminescence (RPL) and thermally-stimulated luminescence (TSL). The RPL is due to the valence change of the Sm ion ($\text{Sm}^{3+} \rightarrow \text{Sm}^{2+}$), induced by X-rays, so the photoluminescence emission by Sm^{2+} appears as a result of irradiation and the intensity increases with the irradiation dose. The emission of Sm^{2+} is due to the 5d–4f transitions. The RPL response seems to be related with the thermally-stimulated luminescence (TSL) on the same samples. The TSL emission is predominantly due to Sm^{2+} , instead of Sm^{3+} , indicating that capture of a hole by Sm^{2+} takes place. As a result of TSL (or heat treatment), Sm^{2+} reverts to Sm^{3+} as the original state. The thermal activation energies have been derived from TSL isothermal analyses, and the obtained values are 1.42, 1.55, 1.65, and 1.74 eV.

1 Introduction

In high-energy radiation measurements, phosphors are often used to convert incident radiation photons to low energy photons (often in the visible spectrum) so that one

can use conventional photodetectors to detect the latter indirectly [1]. A scintillator is a type of phosphor used in radiation measurements, which almost instantly converts the incident radiation to light, and thereby allows in-situ measurements. In contrast, a storage phosphor is another type of phosphor, which can store the incident radiation information (incident radiation intensity or the spatial distribution of radiation). Common applications of storage phosphors include radiographic imaging plates and personnel dosimeter badges.

Storage phosphors used in radiation measurements today may be categorized into three different types, depending on the mechanism involved therein. Such mechanisms are thermally-stimulated luminescence (TSL) [2], optically-stimulated luminescence (OSL) [3], and radio-photoluminescence (RPL). In TSL and OSL, electrons and holes are generated by the incident radiation, and then they are stably and locally captured at trapping centres. Since the amount of charges generated depends on the delivered radiation dose, this state represents the storage of radiation information. Further, these trapped charges can be detrapped by external thermal or optical stimulation and then recombine to emit light. The light emission caused by thermal (or optical) stimulation refers to TSL (or OSL). In RPL, on the other hand, new luminescent centres are generated by irradiation; therefore, photoluminescence (PL) intensity observed after the delivery of radiation represents the amount of absorbed radiation dose [4]. A distinct advantage of RPL over TSL and OSL is that such luminescent centres generated by RPL are typically so stable that one can read out the signal multiple times without the fading of signal. Consequently, we can utilize fluorescent microscopy to readout the spatial distribution of absorbed dose with sub-micrometer image resolution [5, 6]. Despite the high stability of the RPL signal, previous studies on some materials

✉ Go Okada
go-okada@ms.naist.jp

¹ Graduate School of Materials Science, Nara Institute of Science and Technology (NAIST), 8916-5 Takayama, Ikoma, Nara 630-0192, Japan

² Department of Applied Chemistry, Graduate School of Engineering, Tohoku University, 6-6-07 Aoba, Aramaki, Aoba-ku, Sendai 980-8579, Japan

³ Department of Electrical and Computer Engineering, University of Saskatchewan, 57 Campus Dr., Saskatoon, SK S7N5A9, Canada

showed that the RPL signal can be erased by illumination with UV exposure or intentionally heating the sample, and these materials are reusable with good reproducibility [5, 7, 8]. Although RPL has desirable advantages over TSL and OSL, and potential use of new applications such as high-density optical memory, there are only a limited number of materials known to exhibit RPL simply because RPL is a newly recognized phenomenon and there are only a few studies. Some selected RPL materials are: LiF [9], Ag-doped phosphate glasses [10–12], $\text{Al}_2\text{O}_3\text{:C}$, Mg [13], and Sm-doped crystals, glasses, and glass-ceramics [4, 7, 8, 14–17].

The aim of present work is to synthesize and characterize Sm-doped KBr single crystals for potential radiation measurement applications. Previously, we have shown that Sm-doped CsBr single crystals show RPL due to intervalence conversion of the Sm ion ($\text{Sm}^{3+} \rightarrow \text{Sm}^{2+}$), caused by X-ray irradiation [18]. Since KBr, in general, has similar material properties, e.g. crystal structure, valence states, optical band gap energy etc., we expect KBr to also exhibit RPL properties. Moreover, these materials are in a chemical group of alkali halides which forms cubic salts, and they can be fabricated in a microcolumnar plate by simple evaporation techniques [19]; the plate consists of microcolumns of thin alkali halide crystals perpendicular to the plane of the plate. The luminescence light generated in the crystals is guided along the columns so that a high image resolution can be obtained as both scintillator and storage phosphor medium.

2 Experimental procedures

Sm-doped KBr single crystals were synthesized by the Bridgman–Stockbarger technique. Reagent grade powders of SmBr (99.9%) and KBr (99.999%) were mixed in stoichiometric ratio. The amount of Sm added was 0.1 and 0.5 mol% of total mixture. The mixture (4 g) was then loaded into a quartz tube (~8 mm in diameter) heated in vacuum at ~550 K for 1 day in order to evaporate the water content, and eventually the tube was sealed under vacuum to make an ampoule. Further, the quartz ampoule was loaded to a vertical translation furnace, the powder mixture was melted at 1050 K, and the ampoule was slowly translated from the hottest region in the furnace at a rate of 1.0–2.0 mm/h in order to grow the crystal. The thermal gradient measured was about 1.3 K/mm. After the synthesis, the as-grown crystal was cut into disks of approximately 10 mm diameter by 1 mm thickness, and the surfaces were mechanically polished for optical characterization measurements.

Optical transmittance was measured using a spectrophotometer (V-670, JASCO) over the spectral range of

200–700 nm. The PL emission spectrum was measured using a fibre-coupled CCD-based spectrometer (QEPro, Ocean Optics) while the sample was excited with UV light (340 nm). Here, the excitation light was created by inserting a bandpass filter (ZRR0340, Asahi Spectra) into a light beam from a Xenon lamp (LAX-C100, Asahi Spectra). On the other hand, PL excitation spectrum was measured using a spectrofluorometer (FP8600, JASCO). An X-ray generator (XRBOP&N200X4550, Spellman) was used to irradiate a sample to study the radiation induced effects. The X-ray generator was equipped with an ordinary X-ray tube with a W anode and Be window. For all the experiments, the applied anode voltage was fixed to 40 kVp. The representation of X-ray dose used throughout this paper is dose in air at the surface of sample (it is not the deposited dose). TSL glow curve was measured using the following experimental set-up. The sample was placed on a ceramic heater in which the temperature was increased as a ramp at a rate of 1 °C/s using a Sakaguchi temperature controller (SCR-SHQ-A). TSL emission from the sample was then collected by an optical fibre to guide the light into a CCD-based spectrometer (QEPro, Ocean Optics).

3 Results and discussion

Using the Bridgman technique, we have been able to synthesize single crystals of KBr:Sm. Figure 1 shows the transmittance spectra of a typical KBr:0.5%Sm sample as a function of X-ray irradiation dose, whereas the inset shows

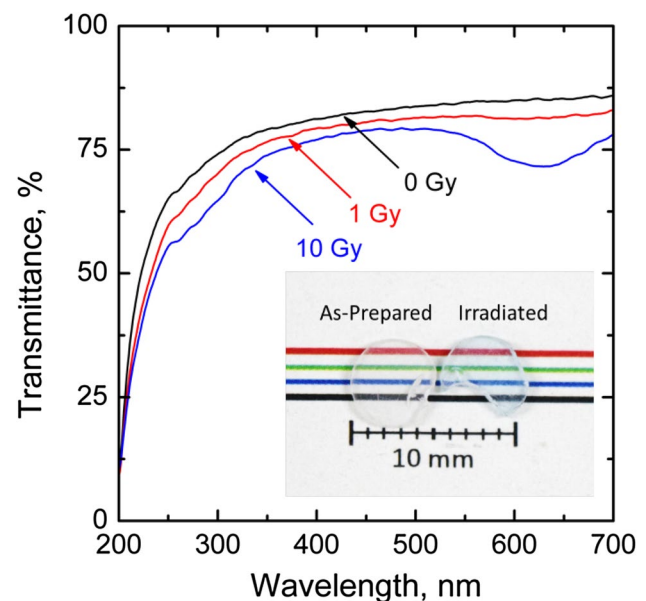


Fig. 1 Transmittance spectra of KBr:Sm as a function of irradiation dose. The inset is a photograph of KBr:Sm single crystal samples before and after being irradiated by X-rays

as-prepared and irradiated sample pieces. The as-prepared sample is shown on the left-hand side of the inset in Fig. 1. The as-prepared sample is colourless and reasonably transparent while the irradiated sample becomes bluish but remains transparent. In the transmittance spectra, this colour change is seen as the appearance of an absorption band around 630 nm, induced by X-ray irradiation. In addition, it seems that there is a weak absorption band induced in the near UV range. A similar absorption band at 630 nm is seen in CsBr due to radiation-induced F^- centres by Br vacancies [19].

Figure 2 compares the PL spectra of KBr:0.5%Sm measured before and after X-ray irradiation (10 Gy). The inset shows the enlarged spectra in the 500–900 nm region. The excitation wavelength is 340 nm. It can be seen that, before the X-ray irradiation, there are very strong emission bands around 415 nm and weak triplet signatures around 565, 600, and 650 nm. The origin of the former emission could not be clearly identified. It should be pointed out that another set of investigations on Eu-doped KBr has also shown an emission at the same wavelength in addition to an emission band of the Eu^{2+} -ion. Therefore, we think that the origin of this emission is strongly related to the host material. The set of line emissions at 565, 600, and 650 nm is typical for the Sm^{3+} ion due to the parity forbidden 4f–4f transitions. Since the 4f electrons are shielded by the outer 5d shell, the electronic structure of the 4f electrons is relatively unchanged, regardless of the host material; thus the 4f–4f transitions are observed at the same wavelengths. The irradiated sample, however, shows different luminescence features. In addition to the emissions mentioned above,

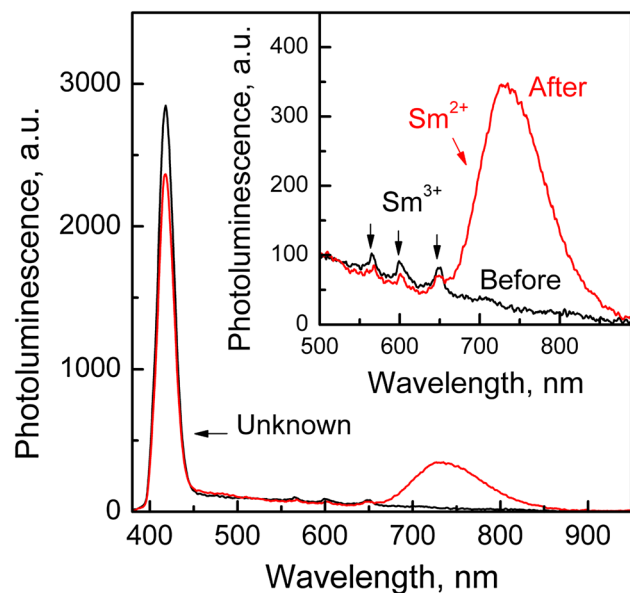


Fig. 2 PL spectra of Sm-doped KBr single crystal measured before and after X-ray irradiation. The excitation wavelength is 340 nm

an intense and broad emission appears in the near infrared region around 730 nm. It should be emphasized that KBr:Sm synthesized in this work can be regarded as a new material that shows RPL properties since a new luminescent centre was generated by X-ray irradiation.

Figure 3 shows the excitation spectra of the emissions in KBr:Sm observed after irradiation. The host-related emission at 420 nm has mainly two excitation bands around 210 and 260 nm. The Sm^{3+} (represented by the 600 nm emission) can be excited below 250 nm and around 270 nm. The former excitation appears as a “tail” and its peak is outside the range of our spectrometer. The optical band gap of KBr is 7.4–7.8 eV [20–22] which corresponds to wavelengths shorter than 170 nm. The 270 nm excitation band may be due to energy transfer from the host to Sm^{3+} ion since the excitation band is similar to what is observed for the host-related emission. Moreover, the weak excitation lines in the 300–450 nm region are due to the typical 4f–4f forbidden transitions of Sm^{3+} . The excitation spectrum of the 720 nm emission (representing Sm^{2+}) is very different from those mentioned above; therefore, the origins are also different. The notable feature is the broad excitation band in the near UV and blue region. The features of broad band excitation in the UV-blue region and broad emission in the near infrared region suggest the origin is due to parity allowed transitions of the Sm^{2+} ion. The earlier study [18] of CsBr:Sm has also shown similar excitation and emission features which were attributed to the Sm^{2+} ion which was reduced from Sm^{3+} by X-ray irradiation. Such reduction of a valence state is in general explained by capturing

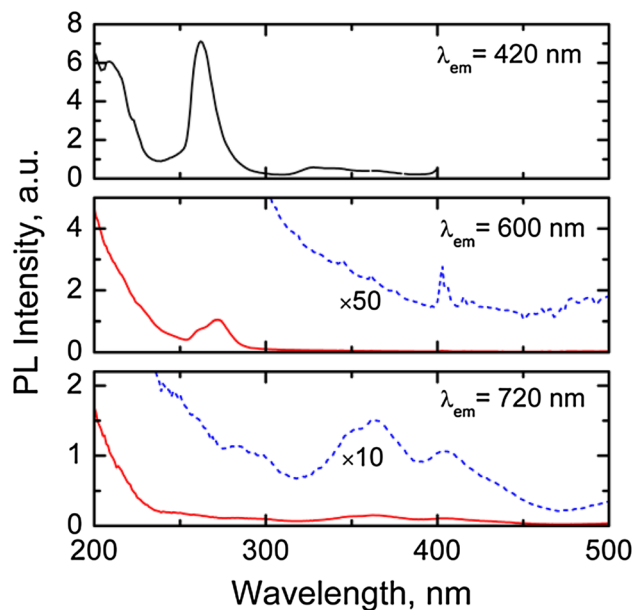


Fig. 3 Excitation spectra of Sm-doped KBr single crystals for emissions at 420, 600, and 720 nm

one of X-ray generated electrons by a Sm^{3+} ion [7, 18, 23]. Therefore, based on the observations above and our current knowledge, we conclude that the RPL observed in KBr:Sm is due to the intervalence conversion of the Sm-ion ($\text{Sm}^{3+} \rightarrow \text{Sm}^{2+}$) caused by X-ray irradiation. It is worth mentioning here that Sm^{2+} could also show luminescence due to 4f–4f transitions which appear as multiple sharp line peaks in the spectrum. In the case of $\text{BaCl}_2:\text{Sm}^{2+}$, both emissions due to the 5d–4f and 4f–4f transitions are observed [24]. The reason is because the excited 5d level is located reasonably above the $^5\text{D}_0$ level (lowest excited level of 4f electrons). In $\text{CaF}_2:\text{Sm}^{2+}$ [17], in contrast, only emission due to the 5d–4f transitions are observed at room temperature since the lowest 5d level is located at the equivalent level of that of the $^5\text{D}_0$ level. In the case of KBr , since only 5d–4f transitions are observed, the energy configuration is expected to be similar to that in CaF_2 .

The top figure in Fig. 4 shows the dose response functions of RPL from 0.1 and 0.5% Sm doped KBr single crystals. The RPL response was defined as follows.

$$\text{Response} = I_1(650-750 \text{ nm}) - I_0(650-750 \text{ nm}) \quad (1)$$

where the former and latter terms are integrated PL intensities over 650–750 nm of irradiated and non-irradiated samples, respectively. For the 0.1%Sm-doped sample, the response increases approximately linearly up to 100 mGy followed by a more gradual but monotonic increase for larger doses. For the 0.5%Sm-doped sample, the response curve consists of two parts as in the first sample; however, the sensitivity is lower and the linear region continues to several hundred milligrays. Therefore, the sensitivity and dynamic range depend on the concentration of Sm-ions. In our experiments, the minimum detectable dose was ~ 1 mGy. However, the instrument was not optimized; especially the photodetector used was a CCD-spectrometer instead of a more sensitive detector such as an APD. Optimizing the reader should increase the sensitivity as a comprehensive system, but this beyond the scope of this work.

The RPL response is reproducible as demonstrated in the bottom figure in Fig. 4. A sample was irradiated with X-rays (1 Gy), and PL was measured to obtain an RPL response. Then, the sample was heated at 300 °C for 5 min in order to erase the signal. The response value slightly deviates for technical difficulties of placing the sample in the same position for each measurement after every annealing process. Detailed experimental data and discussion will follow.

Figure 5 compares the TSL glow curve and RPL response as a function of annealing temperature. The sample used here is 0.5% Sm-doped KBr , and the sample was irradiated to approximately 10 Gy of X-rays before the measurement. The RPL response was measured at room temperature after heat-treatment at a corresponding

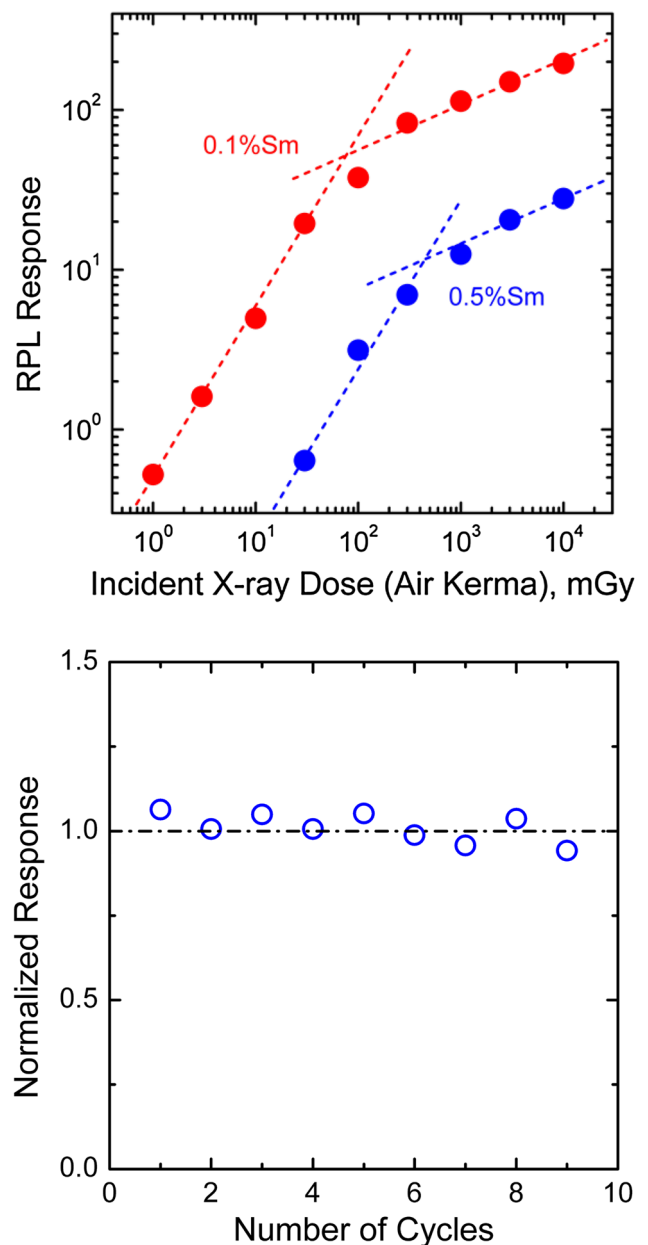


Fig. 4 Dose response functions of RPL in KBr:Sm single crystals (*top*) and demonstration of reproducible RPL response (*bottom*)

temperature. On one hand, it is immediately verified that the TSL glow curve consists of multiple peaks, which implies that multiple charge trapping centres are involved here. On the other hand, the RPL response signal decreases with increasing heat-treatment temperature. These two separate experimental data seems to be well-correlated. Especially the sharp decrease located at around 150 °C and this is the temperature that the main TSL glow peak is seen. As the heat-treatment temperature increases further, eventually the RPL response is completely removed and the TSL signal is not observed in the high temperature range. Figure 6

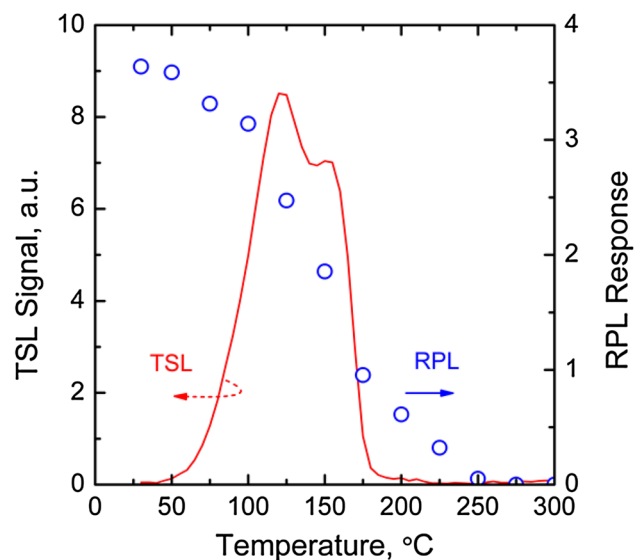


Fig. 5 TSL glow curve and RPL response as a function of heat-treatment temperature. The glow curve was measured from room temperature at a heating rate of 1 °C/s. For RPL measurements, a sample was irradiated at room temperature and heat-treated at the corresponding temperature for ~5 min, and then PL measurement was conducted at room temperature to measure the RPL signal intensity

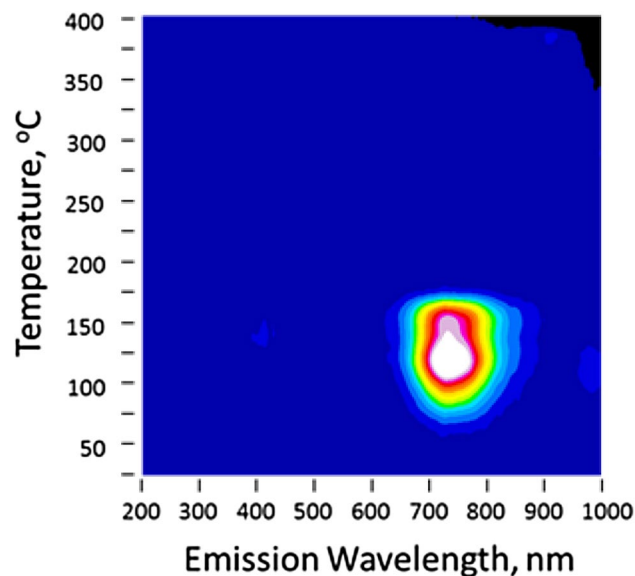


Fig. 6 Contour plot of TSL spectrum as a function of temperature while heating a sample at a rate of 1 °C/s

illustrates a contour plot of the TSL spectrum as a function of temperature. To our surprise, it is clearly apparent that the luminescent centre observed as TSL is mainly due to Sm^{2+} . This indicates that instead of electrons being thermally detrapped from the Sm^{2+} ion, some holes trapped at some centres are first detrapped and then they recombine at

the Sm^{2+} centres (showing the Sm^{2+} emission) followed by the reversed reaction of the Sm-ion ($\text{Sm}^{2+} \rightarrow \text{Sm}^{3+}$).

Charge trapping depths involved in the TSL glow curves shown in Figs. 5 and 6 were characterized by isothermal decay analyses. This approach can be commonly used to extract the information on charge trapping levels [25]. Figure 7 shows isothermal decay curves of 0.5%Sm-doped KBr crystal sample measured at 90, 120, and 150 °C. In these measurements, the sample was placed on a ceramic heater maintained at the desired temperature, irradiated by X-rays until the TSL signal becomes stable with time, and the irradiation was stopped to measure the TSL isothermal decay. The decay curves were best-fitted by the following equation assuming general first order kinetics,

$$I(t) = \sum_{i=0}^n I_i \exp \left[-v_i t \exp \left(-\frac{E_{Ai}}{kT} \right) \right] \quad (2)$$

where $I(t)$ is the isothermal TSL intensity as a function of time t , I_i is initial intensity at $t = 0$, v_i is a frequency factor, E_{Ai} is the activation energy of level i , k is the Boltzmann constant, and T is the sample temperature. Four terms ($n = 4$) were used in the curve fits and the results are summarized in Table 1. The activation energies derived for each decay curve for both 0.1 and 0.5%Sm-doped samples are summarized in Table 1. Since the fitting accuracy of the fastest decay components may not be as good as others, the corresponding values (shallowest trapping centres) are represented with brackets. The analyses showed that

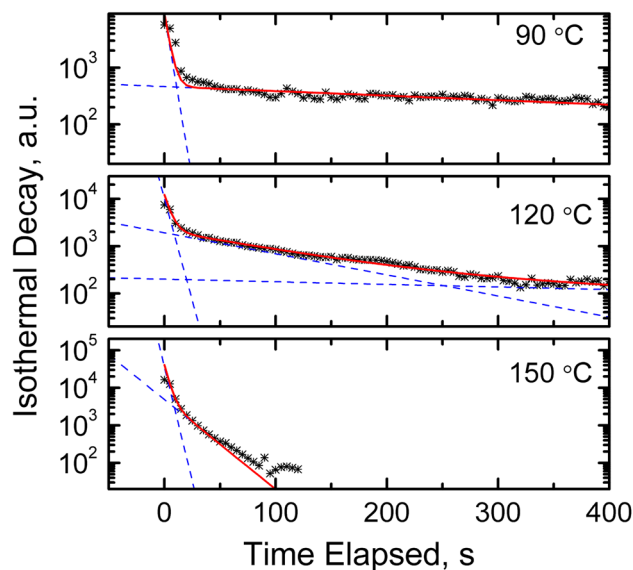
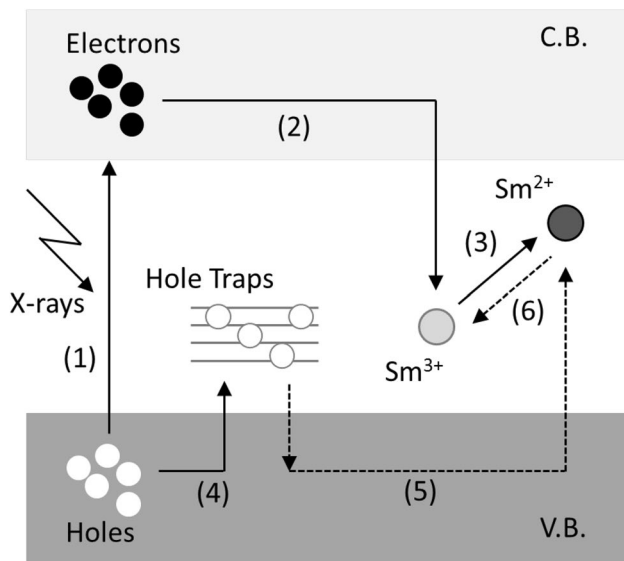


Fig. 7 Isothermal TSL decay curves of KBr:0.5%Sm single crystal at different temperatures. The solid curves are the best fits by Eq. (2), and the dashed lines are exponential components of corresponding charge trapping levels

Table 1 Activation energies E_A (in eV) derived by isothermal TSL decay analyses

Temp. (°C)	Level 1	Level 2	Level 3	Level 4
(a) KBr:0.1%Sm				
90	(1.41)	1.57		
120		(1.54)	1.64	1.71
150			(1.64)	1.70
(b) KBr:0.5%Sm				
90	(1.42)	1.53		
120		(1.55)	1.63	1.83
150			(1.67)	1.73
$E_A = 1.42, 1.55, 1.65, \text{ and } 1.74 \text{ eV}$				

**Fig. 8** Illustration of dynamics involved in RPL and TSL

there are four trapping centres with different activation energies involved in TSL, and the activation energies are reasonably consistent regardless of the doping concentration. The derived activation energies are 1.42, 1.55, 1.65, and 1.74 eV on average for each trapping level respectively.

Figure 8 illustrates the proposed dynamics involved in RPL and TSL of KBr:Sm single crystals based on our experimental analyses in this study. First, the Sm^{3+} -ion is located in the forbidden energy band of the KBr crystal matrix. As a result of interacting with X-rays, electrons and holes are generated (1) and some of the electrons are captured by Sm^{3+} ions (2) and Sm^{3+} becomes Sm^{2+} (3). This was observed by PL measurements. The number of Sm^{2+} ions generated increases with increasing irradiation dose so the PL emission intensity from Sm^{2+} ions also increases with dose. The conversion implies that the X-ray generated holes should be trapped by some centres (deep traps) (4);

however, the exact energy locations of the traps are currently unknown. Next, the generated Sm^{2+} centres can be erased by heating the sample. During the heating process, holes (not an electron at Sm^{2+}) are first detrapped and then recombine with electrons trapped at Sm^{2+} (5), followed by an emission from Sm^{2+} , which then returns back to the Sm^{3+} state (6). This process is interpreted by the fact that TSL was only observed as an emission from Sm^{2+} and nothing else. The TSL isothermal decay analyses revealed that there are probably four different levels of hole trapping centres with the activation energies of: 1.42, 1.55, 1.65, and 1.74 eV.

4 Conclusion

We have synthesized KBr single crystals doped with 0.1 and 0.5% Sm by the Bridgman–Stockbarger technique and characterized their RPL and TSL properties. The samples show RPL as a response to X-ray irradiation dose due to intervalence conversion of the Sm-ion ($\text{Sm}^{3+} \rightarrow \text{Sm}^{2+}$). The X-ray generated luminescence by the Sm^{2+} ion is due to the parity allowed 5d–4f transitions, which appear around 730 nm. The RPL response depends on the concentration of Sm: the sensitivity is higher for the lower concentration. The RPL response (or Sm^{2+} signal) can be erased by heat treatment up to 300 °C. TSL analyses revealed that some trapped holes are thermally detrapped and then recombine with trapped electrons at the Sm^{2+} sites. There are likely to be four different hole trapping centres with activation energies of 1.42, 1.55, 1.65, and 1.74 eV. The erased Sm-doped KBr crystal can be reused and shows reproducible characteristics under further X-ray irradiation, which is very encouraging for potential use as a dosimetric material.

Acknowledgements This research was co-supported by a Grant-in-Aid for Scientific Research (A) (26249147) and Grant-in-Aid for Research Activity start-up (15H06409) from the Ministry of Education, Culture, Sports, Science and Technology of the Japanese government (MEXT). It is also partially supported by the Adaptable and Seamless Technology transfer Program (A-STEP) and Matching Planner Program by the Japan Science and Technology Agency (JST), the Murata Science Foundation, and a cooperative research project of the Research Institute of Electronics, Shizuoka University.

References

1. G.F. Knoll, *Radiation Detection and Measurement*, 4th edn. (Wiley, Hoboken, 2010)
2. S.W.S. McKeever, *Thermoluminescence of Solids* (Cambridge University Press, Cambridge, 1985)
3. E.G. Yukihara, S.W.S. McKeever, *Optically Stimulated Luminescence*. (Wiley, Chichester, 2011)

4. G. Belev, G. Okada, D. Tonchev, C. Koughia, C. Varoy, A. Edgar, T. Wysokinski, D. Chapman, S. Kasap, *Phys. Status Solidi* **8**, 2822 (2011)
5. M.S. Akselrod, A.E. Akselrod, *Radiat. Prot. Dosim.* **119**, 218 (2006)
6. T. Kurobori, Y. Yanagida, Y.Q. Chen, *Jpn. J. Appl. Phys.* **55**, 02BC01 (2016)
7. S. Vahedi, G. Okada, B. Morrell, E. Muzar, C. Koughia, A. Edgar, C. Varoy, G. Belev, T. Wysokinski, D. Chapman, S. Kasap, *J. Appl. Phys.* **112**, 73108 (2012)
8. B. Morrell, G. Okada, S. Vahedi, C. Koughia, A. Edgar, C. Varoy, G. Belev, T. Wysokinski, D. Chapman, R. Sammynaiken, S.O. Kasap, *J. Appl. Phys.* **115**, 63107 (2014)
9. M. Levita, T. Schlesinger, S.S. Friedland, *IEEE Trans. Nucl. Sci.* **23**, 667 (1976)
10. R. Yokota, H. Imagawa, *J. Phys. Soc. Jpn.* **23**, 1038 (1967)
11. Y. Miyamoto, T. Yamamoto, K. Kinoshita, S. Koyama, Y. Takei, H. Nanto, Y. Shimotsuna, M. Sakakura, K. Miura, K. Hirao, *Radiat. Meas.* **45**, 546 (2010)
12. T. Kurobori, W. Zheng, Y. Miyamoto, H. Nanto, T. Yamamoto, *Opt. Mater.* **32**, 1231 (2010)
13. M.S. Akselrod, A.E. Akselrod, S.S. Orlov, S. Sanyal, T.H. Underwood, *J. Fluoresc.* **13**, 503 (2003)
14. G. Okada, B. Morrell, C. Koughia, A. Edgar, C. Varoy, G. Belev, T. Wysokinski, D. Chapman, S. Kasap, *Appl. Phys. Lett.* **99**, 121105 (2011)
15. G. Okada, S. Vahedi, B. Morrell, C. Koughia, G. Belev, T. Wysokinski, D. Chapman, C. Varoy, A. Edgar, S. Kasap, *Opt. Mater.* **35**, 1976 (2013)
16. V. Martin, G. Okada, D. Tonchev, G. Belev, T. Wysokinski, D. Chapman, S. Kasap, *J. Non. Cryst. Solids* **377**, 137 (2013)
17. G. Okada, J. Ueda, S. Tanabe, G. Belev, T. Wysokinski, D. Chapman, D. Tonchev, S. Kasap, *J. Am. Ceram. Soc.* **97**, 2147 (2014)
18. G. Okada, Y. Fujimoto, H. Tanaka, S. Kasap, T. Yanagida, *J. Rare Earths* **34**, 769 (2016)
19. H. Nanto, A. Nishimura, M. Kuroda, Y. Takei, Y. Nakano, T. Shoji, T. Yanagita, S. Kasai, *Nucl. Instruments Methods Phys. Res. Sect. A* **580**, 278 (2007)
20. A.B. Kunz, *Phys. Rev. B* **26**, 2056 (1982)
21. F.C. Brown, C. Gähwiller, H. Fujita, A.B. Kunz, W. Scheifley, N. Carrera, *Phys. Rev. B* **2**, 2126 (1970)
22. R.T. Poole, J.G. Jenkin, R.C.G. Leckey, J. Liesegang, *Chem. Phys. Lett.* **26**, 514 (1974)
23. S. Vahedi, G. Okada, C. Koughia, R. Sammynaiken, A. Edgar, S. Kasap, *Opt. Mater. Express* **4**, 1244 (2014)
24. A. Edgar, C.R. Varoy, C. Koughia, D. Tonchev, G. Belev, G. Okada, S.O. Kasap, H. von Seggern, M. Ryan, *Opt. Mater.* **31**, 1459 (2009)
25. K. Shinsho, Y. Suzuki, K. Harada, Y. Yamamoto, A. Urushiyama, *J. Appl. Phys.* **99**, 0 (2006)